Supplement of Earth Surf. Dynam., 11, 383–403, 2023
https://doi.org/10.5194/esurf-11-383-2023-supplement

Earth Surface Dynamics
Open Access
EGU

Supplement of

Evolution of an Alpine proglacial river during 7 decades of deglaciation

Livia Piermattei et al.

Correspondence to: Livia Piermattei (livia.piermattei@wsl.ch)

S1 Topographic data processing and post-processing of historical and digital aerial images and LiDAR data

Table S1: Attributes of the aerial images. * Only orthophoto is generated.

Acquisition date (aerial image type)	No. processed Photos	Camera Model (Band)	Focal length [mm]	Flying height above terrain [m]	GSD (processed GSD) [m]
8 Sep 1953 (film)	124	Wild RC5 (BW)	210.1	3330	0.23
7 Oct 1969 (film)	23	Wild RC5/RC8 (BW)	152.0	5050	0.45
29 Sep 1970 (film)	32	Wild RC5/RC8 (BW)	210.4	3450	0.19 (0.38)
18 Aug 1971 (film)	39	Wild RC5/RC8 (BW)	209.5	3080	0.16 (0.35)
13 Sep 1982 (film)	34	Wild RC10 (BW)	152.6	6090	0.52
24 Sep 1983 (film)	7	Wild RC10 (BW)	152.6	4840	0.40
10 Oct 1990 (film)	35	Wild RC10 (BW)	152.6	5850	0.53
11 Sep 1997 (film)	25	Wild RC10 (BW)	152.7	6010	0.56
5 Sep 2003 (film)	59	— (RGB)	305.1	4800	0.24
9 Sep 2009 (digital)	142	— (RGB)	—	3200	0.17
31 Jul 2010 (digital)	413	— (RGBN)	—	2870	0.16
18 Jul 2014 (digital)*	819	Hasselblad H3DII-50 (RGB)	—	674	0.07
5 Oct 2015 (digital)*	94	UltraCamX (RGBN)	—	3250	0.18
29-30July 2019	9567	DJI Phantom Pro	—	40-100	0.01-0.10

Table S2: Attributes of LiDAR data.

Acquisition date	**Type**	**Scanner model**	**Wavelength [nm]**	**Operator**	**Average point density* [pts/m²]**
5 Sept 2006	ALS	-	-	Land Tirol	4.9
2008	ALS	-	-	Land Tirol	3.3
4 Jul 2012	ALS	Riegl LMS Q680i-S	1064	Milan Geoservice GmbH (commissioned)	12.7
18 Jul 2012	ALS	Riegl LMS Q680i-S	1064	Milan Geoservice GmbH (commissioned)	12.3
25 Oct 2012	ALS	Riegl LMS Q680/400	1550	Milan Geoservice GmbH (commissioned)	9.6
18 Jul 2014	ALS	Riegl LMS VQ580	1064	Milan Geoservice GmbH (commissioned)	9.6
10 July 2015	ALS	-	near infrared	-	20.2
22 Aug 2015	ALS	-	near infrared	-	38.0
5 Jun 2017	ALS	Riegl VuxSys-LR	1550	Chair of Physical Geography University of Eichstätt-Ingolstadt	19.9
25 June 2019	TLS	VZ-4000/Riegl	near infrared	Chair of Physical Geography University of Eichstätt-Ingolstadt	222

The “Amt der Tiroler Landesregierung” (https://www.tirol.gv.at/en/) and the “Bundesamt für Eich- und Vemessungswesen” (BEV) (https: //www.bev.gv.at) provide the historical aerial photographs as scanned images in tiff format with jpeg compression. The scanning resolution is 15 μm with the exception of the 1970 and 1971 datasets, which are scanned at 12 μm. The historical aerial images covered 8 periods from 1953 to 2003 (Table S1). The scanned images are processed with the Agisoft Metashape software and a comparison is made with the Inpho software with the 2003 dataset used in this work. The Metashape v1.5 software can process the film camera using fiducial marks. Note that cropping the image is a necessary step because each image must have the same number of pixels in order to be recognized as having been acquired by the same camera and consequently share

the same calibration parameters. Black border masking is not required but is recommended because it can interfere with the orientation of the camera. For the orientation, the number of key and tie points is set to zero to have the maximum number of detectable feature points; orientation is performed at full image resolution (called ultra-high in the software). Despite the availability of the calibration protocol, it is preferred not to keep the calibration parameters fixed during orientation and bundle adjustment. However, this functionality must be verified. The camera optimization parameters include the focal length, the fiducial centre, and radial and tangential distortion. The GCPs used for co-registration and camera optimization were selected from the 2017 LiDAR point cloud (Fig. S1 bottom right), with an estimated horizontal and vertical accuracy of approximately 25 cm.

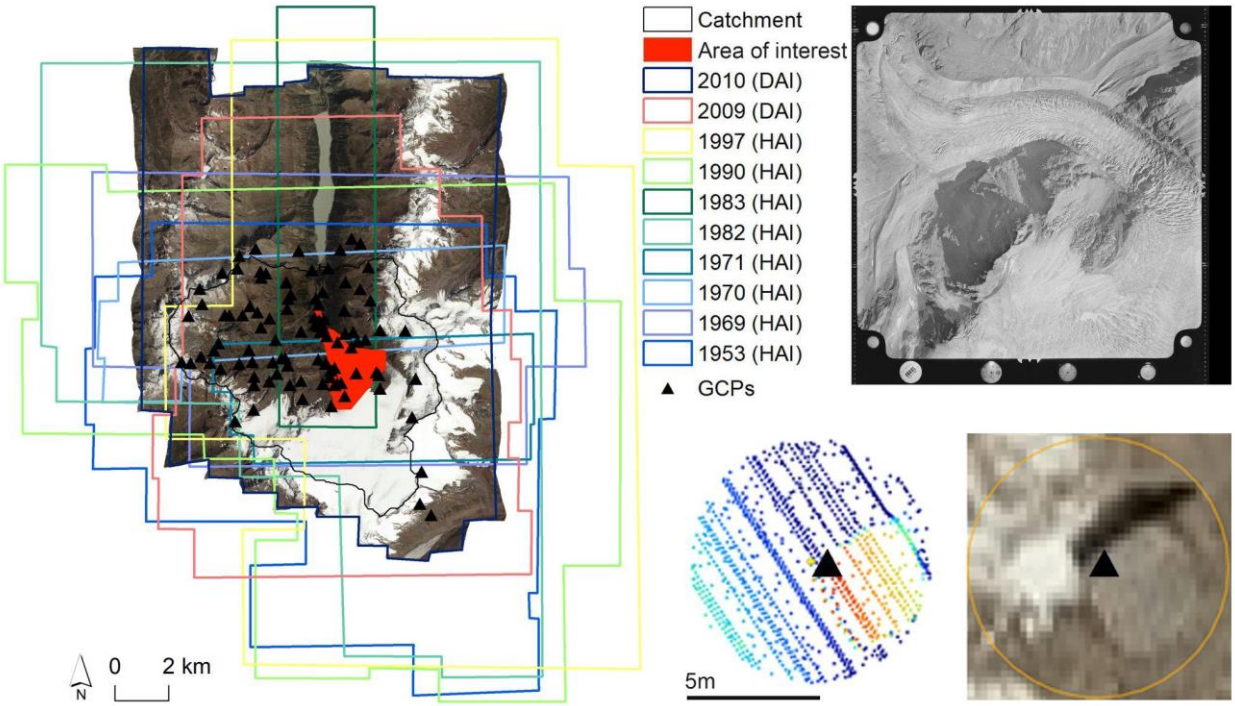

Figure S1: On the left, images footprint of historical (HAI) and digital (DAI) aerial images for each aerial flight with the location of the GCPs overlaid to the 2010 orthophoto. The selection of one GCP on the reference 3D ALS 2017 point cloud colored by elevation and its corresponding location on the 2010 orthophoto is shown on the bottom right. On the top right, a scanned image of the 1953 aerial flight photographing the glacier tongue.

GCPs were evenly distributed throughout the entire catchment (Fig. S1). However, a large number of GCPs were identified within the area of interest with approximately 15 GCPs per stereo pair.

Additional digital aerial images provided by BEV were collected in 2009 and 2010 with RGB and NIR information. Available aerial images from 2014 and 2015 from the “Amt der Tiroler Landesregierung" are processed in order to generate high-resolution orthophotos. The processing of the aerial images as well as the UAVs images did not involve any data preparation and thus processing begins with camera orientation followed by GCPs selection and bundle block adjustment, dense cloud generation, and export of the orthophoto. Note that the same GCPs adopted for the historical images were also used for these datasets. Dense image matching was performed at half the resolution of the images to reduce calculation time and file size.

The companies that collected the data (see Table S2) provided all the airborne LiDAR point clouds, with the exception of the 2017 Lidar data was collected by us. We used a Riegl VuxSys-LR integrated into a helipod, mounted on a Eurocopter AS350-B3 Ecureil helicopter. The entire Kaunertal catchment was scanned along a total of 50 profile lines at a flight altitude of approximately 150 meters. The recorded raw trajectory was processed with a GNSS recording base station within the Kaunertal, located at the Weißseeferner (Applanix Pospac), and linked

to the raw LiDAR data in the Riegl Riprocess software. In Riprocess, an initial fine referencing of the individual flight strips was carried out with the reprocessing tool before the final strip adjustment. For the collection and processing of TLS data, please refer to Altmann et al. (2020).

All the photogrammetric and ALS point clouds are co-registered with the ALS 2017 point cloud before raster interpolation. The post-processing workflow from point cloud to DEM generation is shown in Fig. S2.

A stable area mask corresponding to the year 2015 is generated using the RGBNIR orthophoto (Figure S3). This mask is then adjusted for each epoch by removing (i) the glacier extent, (ii) any snow patches, and (iii) all pixels with an absolute height difference with the reference ALS 2017 greater than 1 m (for historical DEMs) and 0.50 m (for all DEMs after 2003). ICP co-registration is performed using Opals Module ICP. The point clouds were then interpolated into a raster using a robust moving window. . The raster resolution was 1 m for the archive aerial images (from 1953 to 2003) and 0.5 m for the remaining DEMs. Gaps in the raster were filled with a moving plane interpolation with inverse distance weighting. The uncertainty estimation of each DEM was performed on the same stable area used for the ICP co-registration by means of a DEM of differences between the slave DEM and the reference DEM (ALS 2017).

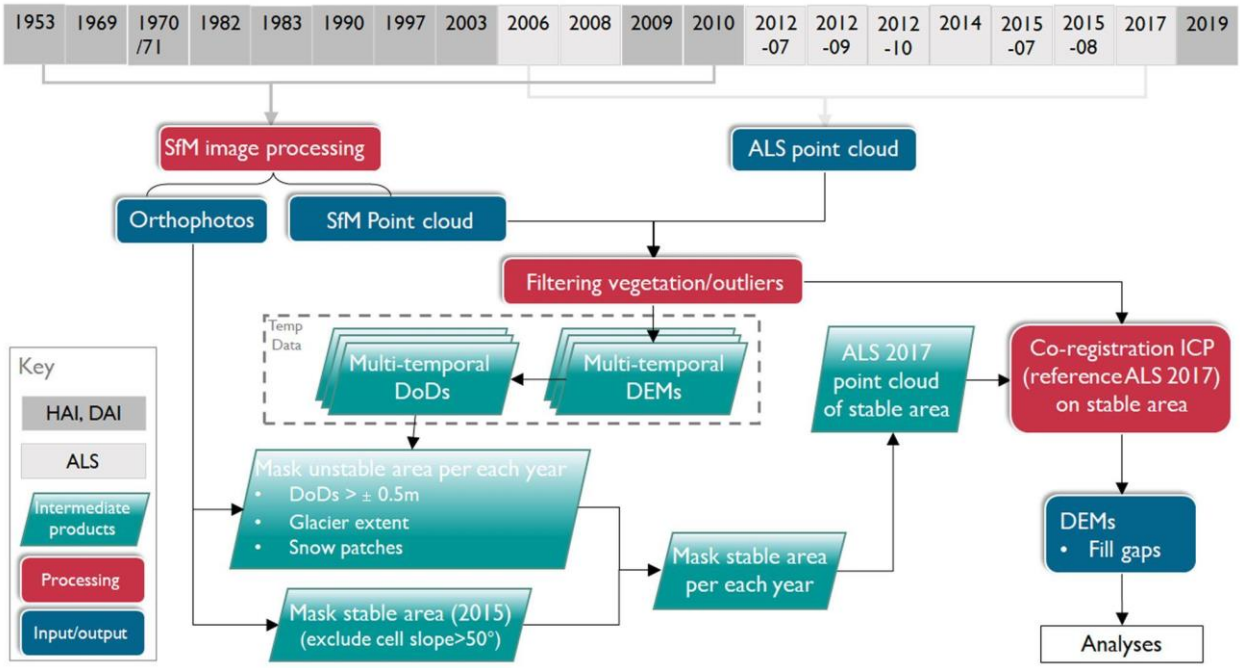

Figure S2: Diagram of the post-processing workflow of 3D point cloud from ALS and historical and digital aerial images (HAI & DAI). Red and blue rectangles show the processes, and the input/outputs data, respectively, and the trapezoids indicate intermediate products.

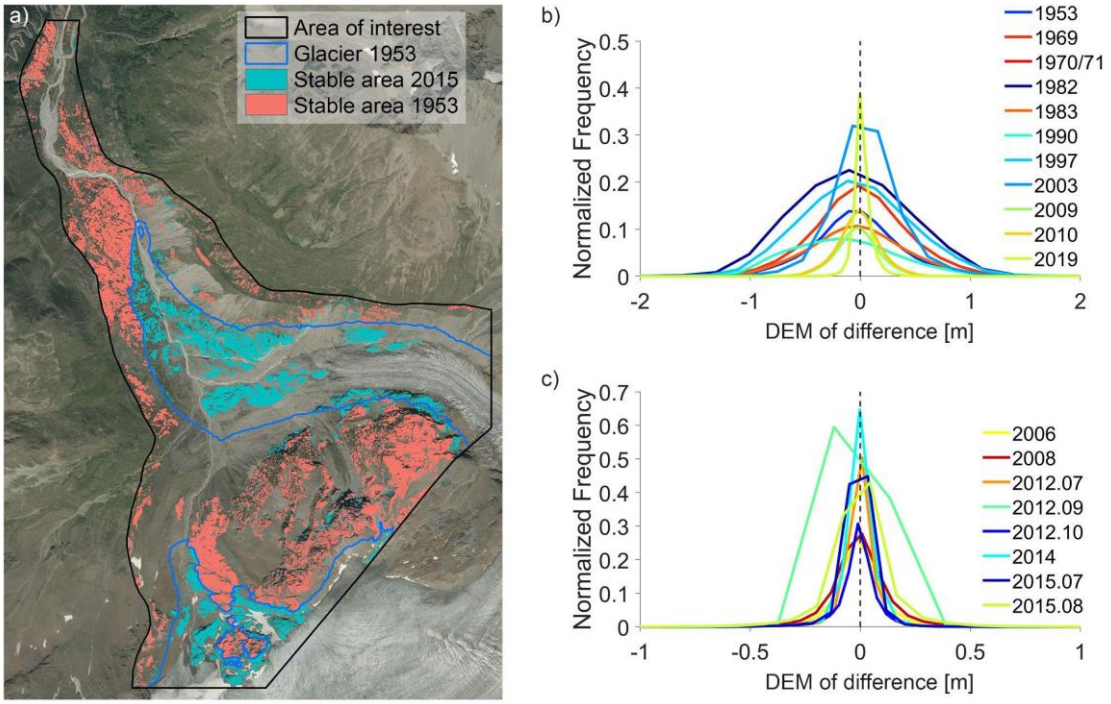

Figure S3: a) Mask of stable area for the year of 1953 and 2015 used for DEM co-registration and the normalized histogram of the elevation difference (DEM of difference) of b) the photogrammetric and c) LiDAR DEMs with respect to the reference ALS 2017.

Table S3: Elevation difference in meters with the reference ALS 2017 DEM over the stable area. The σ_{MAD} is used for uncertainty estimation.

$Year_{DEM}$	Elevation difference with the reference ALS 2017 DEM [m]						
	Min	Max	Mean	σ	Median	RMSE	σ_{MAD}
1953	-7.09	5.06	-0.03	0.40	-0.04	0.40	0.31
1969	-9.78	8.81	0.01	0.43	0.00	0.43	0.33
1970	-34.42	4.40	-0.01	0.32	-0.01	0.32	0.23
1982	-21.73	8.52	-0.08	0.52	-0.09	0.53	0.41
1983	-6.89	4.28	-0.02	0.44	-0.03	0.44	0.35
1990	-6.31	3.62	-0.16	0.48	-0.18	0.51	0.39
1997	-19.65	5.24	-0.04	0.49	-0.05	0.49	0.39
2003	-19.32	3.46	0.06	0.31	0.05	0.31	0.22
2006	-3.30	2.40	-0.01	0.12	-0.01	0.12	0.08
2008	-4.34	2.62	0.00	0.13	-0.01	0.13	0.09
2009	-2.38	2.31	-0.02	0.20	-0.02	0.21	0.16
2010	-3.71	2.21	-0.02	0.20	-0.01	0.20	0.15
2012.07	-3.66	2.72	-0.01	0.08	0.00	0.08	0.05
2012.09	-20.48	4.81	-0.01	0.10	0.00	0.10	0.05
2012.10	-2.18	2.12	-0.01	0.10	-0.01	0.10	0.06
2014	-4.01	4.43	0.00	0.08	0.00	0.08	0.05
2015.07	-4.92	3.41	-0.01	0.08	-0.01	0.08	0.05
2015.08	-5.43	6.60	0.00	0.16	0.00	0.16	0.09
2019	-1.94	3.17	0.02	0.11	0.01	0.11	0.06
2019	-2.26	1.82	0.03	0.12	0.01	0.12	0.06

S2 Sediment volume of active floodplains and lateral hillslopes

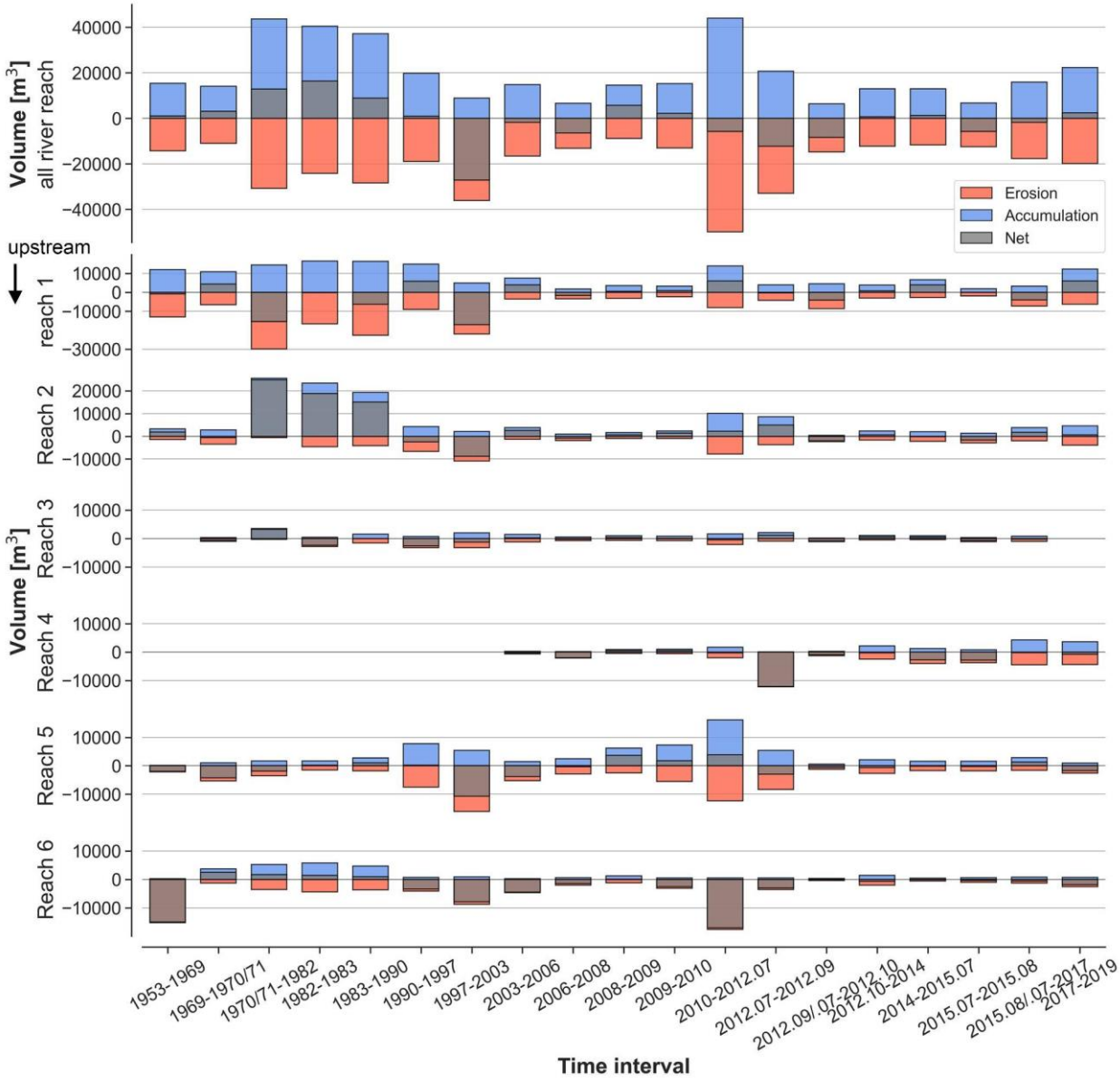

Figure S4: Visualization of the sediment volume of all connected active floodplains (i.e. "all river reaches") and for each river reach for each time step. Note that due to glacier retreat reaches 4, 5 and 6 are connected to downstream river reaches from 2003 onwards. Therefore, the total volume of the first time step (1953-1969) is only composed of river reaches 1 and 2; river reach 3 is included in the total volume from the second time step onwards.

Table S4: For each time step the area change of the active floodplain, the sediment volume estimation, the sigma volume (σ_v) (i.e. the σ_{MAD} derived with respect to ALS 2017 DEM (Table S1) multiplied by the area) and the net volume rate. Elevation difference on stable terrain between consecutive DEMs and their common stable terrain is also reported.

Time step	DEM of difference on stable terrain consecutive DEMs			Area active channel	Volume erosion	Volume deposition	Net Volume	σ_v	Net volume rate
	Common Stable Area [m²]	*Mean* [m]	σ [m]	[m²]	[m³]	[m³]	[m³]	[m³]	[m³ yr⁻¹]
1953-1969	530430	-0.06	0.49	103346	-14335	15396	1061	46792	66
1969-1970/71	630395	0.02	0.46	120654	-10972	14082	3110	48532	1555

1970/71-1982	497210	0.08	0.58	120521	-30793	43638	12845	56658	1168
1982-1983	438541	-0.07	0.56	118786	-24120	40517	16398	64035	16398
1983-1990	428281	0.18	0.58	115894	-28335	37202	8866	60731	1267
1990-1997	435792	-0.16	0.54	123833	-18903	19813	910	68299	130
1997-2003	586418	-0.09	0.52	129704	-36048	8938	-27110	58078	-4518
2003-2006	807194	0.06	0.30	131912	-16557	14764	-1793	30880	-598
2006-2008	915237	0.00	0.12	133945	-13102	6641	-6461	16129	-3230
2008-2009	900209	0.02	0.18	136164	-8832	14608	5776	24996	5776
2009-2010	904266	-0.01	0.15	138860	-13079	15303	2224	30454	2224
2010-2012.07	923270	-0.01	0.19	149740	-49815	44055	-5760	23676	-2880
2012.07-2012.09	541637	0.00	0.08	154528	-32961	20762	-12199	10927	-12199
2012.09-2012.10	439991	0.01	0.20	154353	-14752	6436	-8317	12055	-8317
2012.10-2014	728849	-0.01	0.22	160594	-12286	12956	670	12543	335
2014-2015.07	1002517	0.00	0.06	161352	-11666	13003	1337	11409	1337
2015.07-2015.08	820669	0.00	0.09	160617	-12440	6689	-5751	16537	-5751
2015.08-2017	1071731	0.00	0.16	164386	-17691	15908	-1783	17781	-891
2017-2019	122925	0.02	0.11	172072	-19874	22281	2407	10324	1204

Table S5: Sediment volume estimation for selected time steps of hillslope 1 and hillslope 2 connected to river reach 2 and 5, respectively.

	Lateral Hillslope 1 connected to river reach 2						**Lateral Hillslope 2 connected to river reach 5**					
Time step	Area	Volume erosion	Volume deposition	Net volume change	σ_v	Net volume change rate	Area	Volume erosion	Volume deposition	Net volume change	σ_v	Net volume change rate
	[m^2]	[m^3]	[m^3]	[m^3]	[m^3]	[m^3 yr^{-1}]	[m^2]	[m^3]	[m^3]	[m^3]	[m^3]	[m^3 yr^{-1}]
1953-1971	35666	-119903	11205	-108698	13767	-6054	–	–	–	–	–	–
1971-1982	128996	-148605	89725	-58880	60642	-5314	–	–	–	–	–	–
1982-1997	127191	-118527	73736	-44791	71973	-2974	47800	-45606	24429	-21177	27048	-1406
1997-2003	133892	-99997	15804	-84193	59953	-14194	56898	-27087	8250	-18836	25477	-3176
2003-2008	135306	-34642	15462	-19180	32162	-3840	56203	-11274	3686	-7588	13359	-1518
2008-2012.07	132425	-16288	9569	-6719	13634	-1732	53606	-18663	3694	-14970	5519	-3742
2012.07-2017	131919	-15496	10002	-5494	6596	-1125	52337	-9992	3725	-6267	2617	-1253

S3 Water mapping of the active floodplain

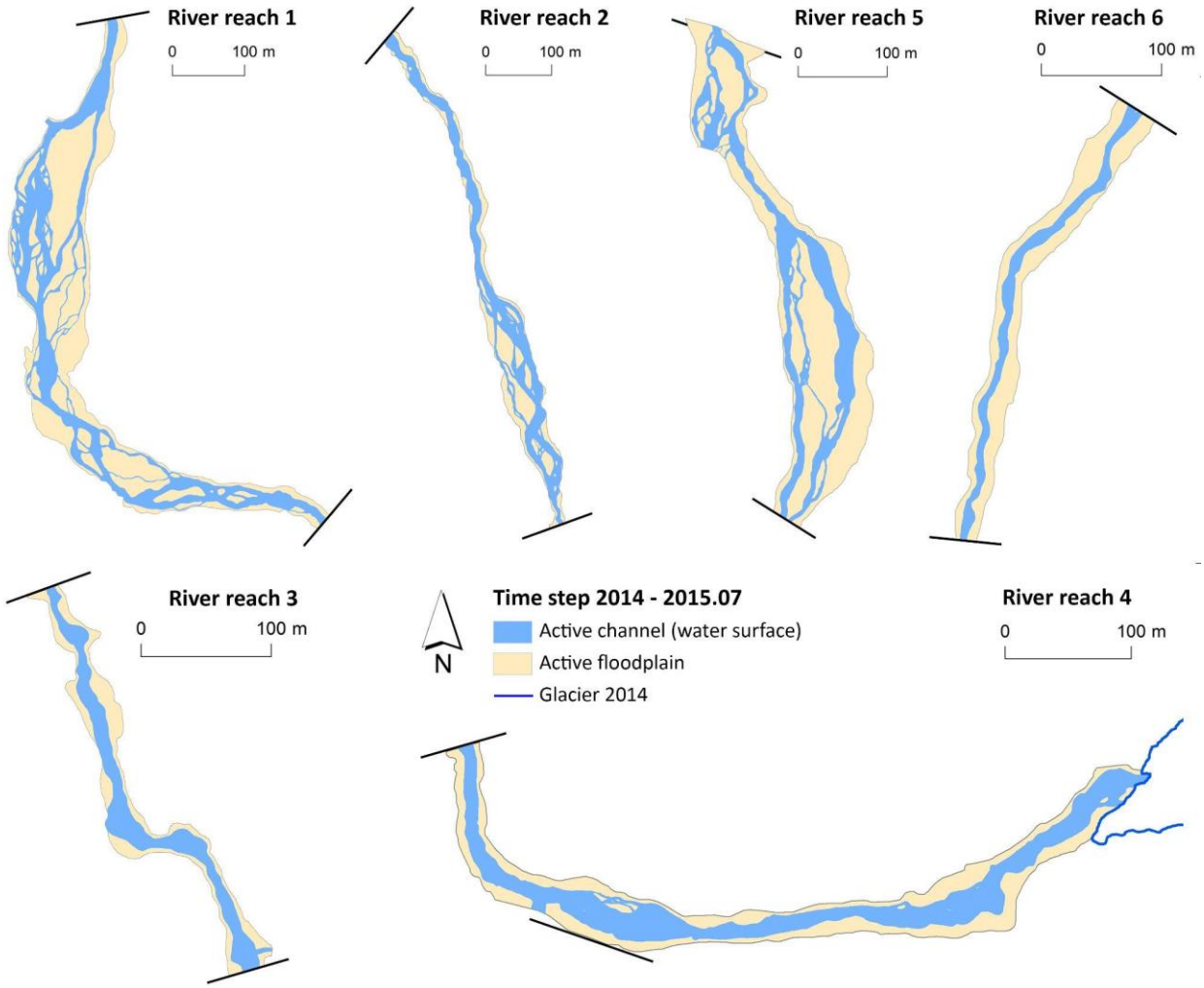

Figure S5: The mapping of the active floodplain and active channel (i.e. the water surface) for every river reach for the time step 2014-2015 July.